Journal of Solid State Chemistry 187 (2012) 316–322

Contents lists available at SciVerse ScienceDirect

Journal of Solid State Chemistry

journal homepage: www.elsevier.com/locate/jssc

Enhanced thermoelectric performance in zinc substituted p-type filled skutterudites $CeFe_{4-x}Zn_xSb_{12}$

Gangjian Tan, Shanyu Wang, Han Li, Yonggao Yan, Xinfeng Tang*

State Key Laboratory of Advanced Technology for Materials Synthesis and Processing, Wuhan University of Technology, Luoshi Road 122#, Hongshan district, Wuhan 430070, People's Republic of China

ARTICLE INFO

Article history:
Received 8 October 2011
Received in revised form
16 January 2012
Accepted 23 January 2012
Available online 30 January 2012

Keywords:
Zn substitution
Filled skutterudite
Thermoelectric property

ABSTRACT

In this study, Zn-substituted polycrystalline skutterudites $CeFe_{4-x}Zn_xSb_{12}$ ($x=0$, 0.05, 0.1, 0.2, 0.3) were successfully prepared by a traditional melting–annealing method. The solubility of Zn in Fe site is ~1.2%, exceeding which trace amount of ZnSb phase can be detected in the XRD. This ZnSb impurity phase, with size of several hundred nanometers for the sample with $x=0.2$ but showing surprisingly small size of ~10 nm for the sample with $x=0.3$, selectively distributes on the grain boundaries. In particular, the introduction of Zn in Fe site effectively improves the Seebeck coefficient in a manner of enhancement in hole effective mass, but it has negligible influence on both electrical and thermal conductivities though the hole concentration is increased. Consequently the corresponding improvement in power factor leads to an improved thermoelectric figure of merit (ZT) of 0.9 at 800 K for the sample with $x=0.1$, which is ~15% higher than that of Zn-free sample. This study demonstrates a favorable effect of Zn iso-substitution and opens a new strategy to improve the thermoelectric properties of p-type Fe-based skutterudites beyond the sole phonon engineering.

Crown Copyright © 2012 Published by Elsevier Inc. All rights reserved.

1. Introduction

Skutterudites are recognized as a highly promising and deeply researched class of compounds in the past 15 years. The original thermoelectric skutterudite $CoSb_3$ has a very high power factor, but its high lattice thermal conductivity largely depresses the overall thermoelectric performance [1]. Filling the voids in the ideal binary structure with electronpositive elements (including lanthanide, actinide, alkaline-earth, alkali, thallium, and group IV elements [2–12]) to produce so-called filled skutterudites has proven to be an effective way to improve the thermoelectric performance with both n-type and p-type compositions. The main characteristic of filled skutterudites is the significantly declined lattice thermal conductivity by "rattling" effect, making them as a promising candidate for intermediate temperature thermoelectric power generation application.

Among various p-type Fe-based filled skutterudites, Ce fully-filled $CeFe_4Sb_{12}$ compound is extensively studied owing to its very low thermal conductivity [1,2,13]. The much lower Seebeck coefficient in comparison to that of the optimized n-type skutterudites [3,9], however, responses to a very low power factor and thus a low $ZT<1.0$. Generally, doping in the Fe site with trivalent Co or tetravalent Ni is an efficient route to enhance the Seebeck coefficient via decreasing the carrier concentration [14–16], which conversely leads to a decrease in the electrical conductivity and apparent bipolar contribution to the thermal conductivity at elevated temperature [15]. Consequently, the overall improvement in ZT value is seldom realized through simple carrier concentration engineering. However, isoelectronic alloying in Fe site which does not introduce significant variation in carrier concentration and deterioration in electrical conductivity provides an alternative way to optimize the electrical transport properties through improving the Seebeck coefficient, under the consideration of enhancement in hole effective mass. By alloying isoelectronic Ir at Co site in the $Ba_{0.3}Co_4Sb_{12}$ skutterudite, the significant increase in Seebeck coefficient leads to a markedly improved power factor, which is mainly due to the increased effective mass [17,18]. The similar result is also obtained in slight Cd-substituted β-Zn_4Sb_3 system [19]. Though Ru substitution for Fe may be a better choice, its mixed valence states would be a confusing issue to deal with [20,21].

In particular, the divalent Zn atom is supposed to be a potential candidate for substituting Fe [22]. Herein, we have investigated the effects of Zn isoelectronic alloying on electrical and thermal transport properties of $CeFe_4Sb_{12}$ skutterudite, and expected to extract some information to explain the origin of improvements in effective mass and Seebeck coefficient.

2. Experiment

Polycrystalline samples with nominal compositions $CeFe_{4-x}Zn_xSb_{12}$ ($x=0$, 0.05, 0.1, 0.2, 0.3) were prepared as follows. Stoichiometric quantities of the constituent pure elements Ce

* Corresponding author: Fax: +86 27 87860863.
E-mail address: tangxf@whut.edu.cn (X. Tang).

0022-4596/$ - see front matter Crown Copyright © 2012 Published by Elsevier Inc. All rights reserved.
doi:10.1016/j.jssc.2012.01.045

Table 1
The room-temperature carrier concentrations[a] (N_p), carrier motilities (μ_H), electrical conductivity (σ), Seebeck coefficients (α) and calculated carrier effective mass m^b/m_e of the $CeFe_{4-x}Zn_xSb_{12}$ bulk samples.

x	Relative density[b] (%)	α (μV/K)	α (10^4 S/m)	$N_p/10^{20}$ cm^{-3}	μ_H /cm^2 V^{-1} s^{-1}	m^b/m_e
0	98.8	84.2	20.66	3.01	38.4	1.89
0.05	99.1	85.9	20.74	3.89	31.3	2.29
0.1	99.1	84.0	20.76	4.11	29.4	2.32
0.2	98.9	80.9	21.25	4.56	29.2	2.40
0.3	98.8	85.7	20.45	5.38	20.3	2.83
ZnSb [24]		196	0.91	6.3E-2	94	

[a] The relative error of measured carrier concentration is ~8%.
[b] The theory density is adopted as 7.9 g/cm^3 for $CeFe_4Sb_{12}$.

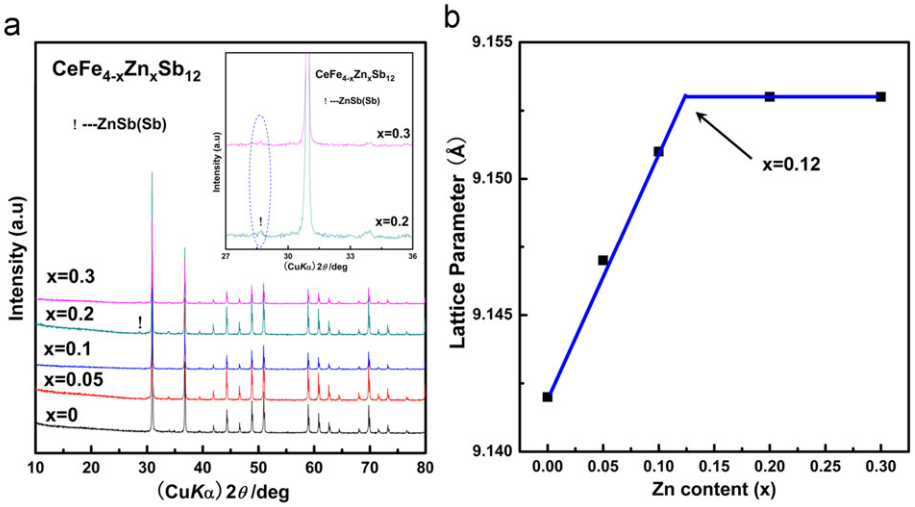

Fig. 1. (a) The powder XRD patterns and (b) the lattice parameters for the $CeFe_{4-x}Zn_xSb_{12}$ compounds.

(99.99%, plate), Fe (99.999%, shot), Zn (99.999%,shot), and Sb (99.9999%, ingot) were weighed according to their nominal composition, loaded into a quartz tube with carbon depositing on the inner wall, and sealed in vacuum under a pressure of 10^{-3} Pa. All the above procedures were done in a glove box filled with high-purity Ar ($O_2 < 0.1$ ppm, $H_2O < 5$ ppm). The samples were slowly heated to 1373 K and rested for 24 h. They were then quenched in a saltwater base and annealed at 953 K for 168 h. The resulting ingots were ground into fine powders and then sintered into dense bulk pellets with size of Φ15 mm by spark plasma sintering (SPS) at 873 K for 5 min under pressure of 40 MPa.

The phase compositions of bulk samples were determined by powder X-ray diffraction (XRD) (PANalytical X'Pert Pro X-ray diffraction) using Cu K_α radiation ($\lambda = 1.5406$ Å) and DSC (TA Instrument, Q20, heating rate 20 K min^{-1} and sample mass 100 mg). The microstructure was investigated by field emission scanning electron microscopy (FESEM, Hitachi, S-4800) and high-resolution transmission electron microscopy (HRTEM; JEM-2100F), The chemical compositions were determined by energy dispersive X-ray spectroscopy (FESEM-EDS, Hitachi, S-4800). The Hall coefficient (R_H) and electrical conductivity (σ_H) at room temperature were measured by Accent HL5500PC Hall system using the van der Pauw method with the magnetic field strength of 0.513 T, and the corresponding carrier concentration (n) and carrier mobility (μ_H) were calculated by the followed equations: $n = 1/e|R_H|$ and $\mu_H = \sigma/ne$. Electrical conductivity (σ) and Seebeck coefficient (α) were simultaneously measured by commercial equipment (ZEM-1, Ulvac Riko, Inc.) under a low pressure inert gas (He) atmosphere from 300 K to 800 K. The thermal conductivity (κ) was calculated from the measured thermal diffusivity (D), specific heat (C_p), and density (d) using the relationship $\kappa = D \times C_p \times d$. The thermal diffusivity was tested by the laser flash diffusivity method using a Netzsch LFA 457 system and the specific heat (C_p) was measured by TA instrument: DSC Q20. All the measurements were performed in the temperature range from 300 K to 800 K. The densities of the bulk samples were measured by the Archimedes method and the relative densities for all samples are higher than 98%, as shown in Table 1.

3. Results and discussion

3.1. Phase composition and microstructure

Fig. 1(a) displays the powder XRD patterns for bulk materials with different Zn content in the titled bulk samples after SPS. Perfect single phases with skutterudite structure can be obtained for the samples with $x \leq 0.1$ and all the diffraction peaks can be indexed to be $CoSb_3$ (JCPDS Card 51-0824). However, as shown in the inset of Fig. 1(a), some trace amount of impurity phases, probably ZnSb or Sb, can be detected in the XRD reflections (near 29°) for the samples with $x = 0.2$ and 0.3. It is worth noting that these peaks tend to become weaker and wider when x increases from 0.2 to 0.3, which is mainly attributable to the decrease in the geometrical size of the impurity phase with increasing Zn content (see the FESEM photos shown below). The lattice parameters of the bulk samples as a function of x is displayed in Fig. 1(b), and it is obvious that the lattice parameter linearly increases from 9.142 Å to 9.153 Å with x increasing up to 0.1, roughly obeying

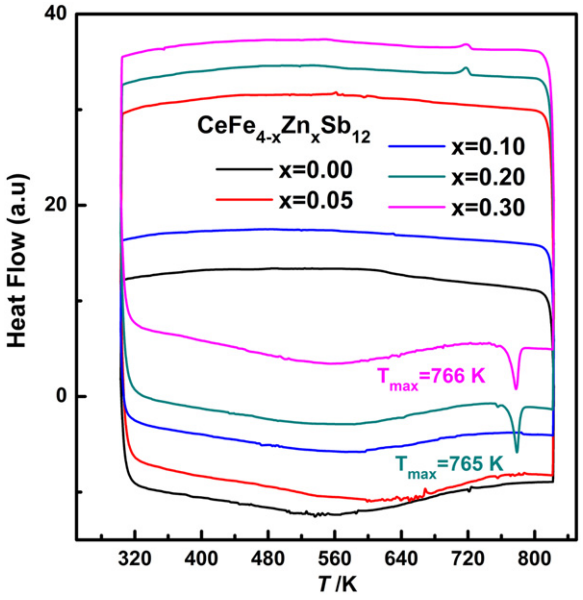

Fig. 2. DSC curves of $CeFe_{4-x}Zn_xSb_{12}$ compounds.

the Vegard's law (indicated by the solid line). The expansion of the lattice mainly arises from the successful substitution of larger Zn atoms at Fe sites. Whereas, the lattice parameter a remains almost unchanged with x further increasing, which means that Zn exceeds solubility limit at such a substitution level. By fitting the plot, we can deduce that the solubility limit of Zn in $CeFe_{4-x}Zn_xSb_{12}$ samples is near 0.12.

To further identify the phase composition of the obtained samples (as evidenced in XRD patterns), the DSC heat flow curves were measured and plotted in Fig. 2. There is no endothermic or exothermic peak for the samples with $x \leq 0.1$ in the whole measured temperature range, which manifests a pure phase and is consistent with the XRD results. An endothermic peak around 765 K, however, can be detected for the samples with $x \geq 0.2$, which is associated with the peritectic reaction of ZnSb compound [23].

Fig. 3 displays the microstructures of the fracture bulk samples. All the samples show clear grains with the average grain size of about 5–10 μm as shown in Fig. 3(a)–(c) and (e) for the samples with $x=0$, 0.1, 0.2 and 0.3, respectively. Two areas M and N, as shown in Fig. 3(b), are randomly selected to determine their chemical compositions by EDS. The compositions are almost identical for the two selected areas, as can be seen in Fig. 4(a) and (b), which reveals that

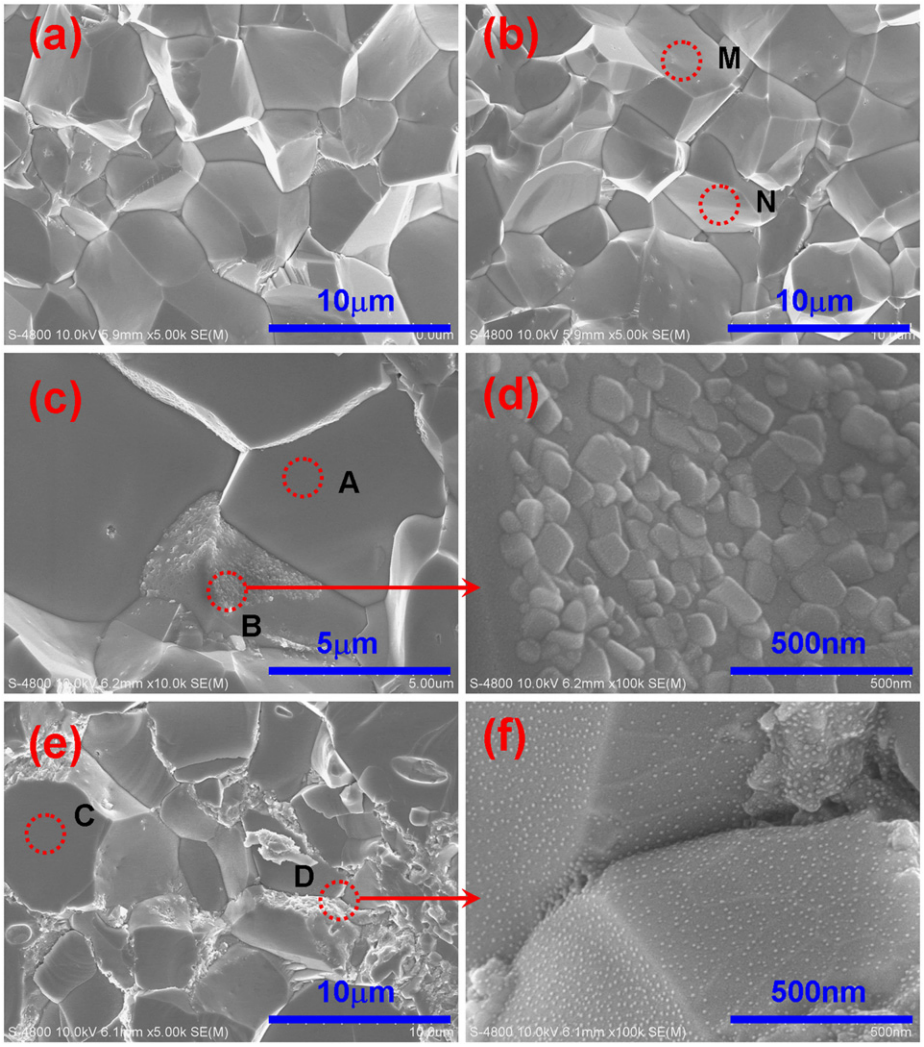

Fig. 3. The FESEM figures of the free-crack surfaces of $CeFe_{4-x}Zn_xSb_{12}$ compounds. (a) $x=0$; (b) $x=0.1$; (c) $x=0.2$; (e) $x=0.3$. (d) and (f) are the enlarged areas for B and D in the figure (c) and (e), respectively.

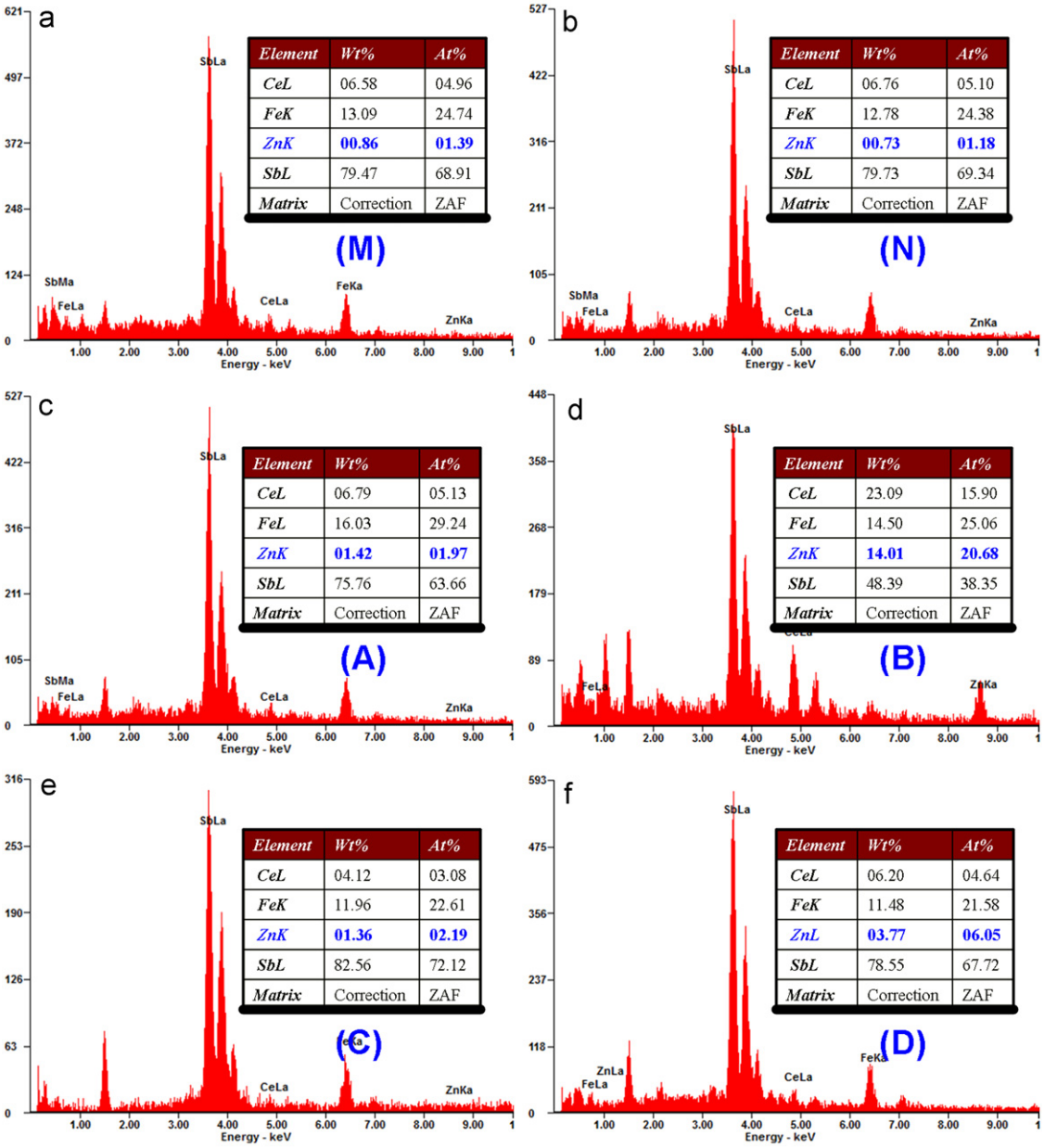

Fig. 4. The EDS results of $CeFe_{4-x}Zn_xSb_{12}$ compounds. **(a)–(f)** corresponds to M,B,C,D areas shown in Fig. 3, respectively.

the compositions of the samples with low Zn content are homogeneous. However, as shown in Fig. 3(c) and (e), some distinct regions with rough surface (*B* and *D* areas) can be observed when x exceeds 0.1. The corresponding EDS measuremnets demonstrate that these areas are rich in Zn element, as shown in Fig. 4(c)–(f). In addition, from the high resolution figures shown in Fig. 3(d) and (f), we can clearly observe some unique nanostructures, showing as 50–200 nm pellets adherent in the interfaces for the sample with $x=0.2$ and surprisingly ~10 nm nanodots for the sample with $x=0.3$. To further ascertain the chemical compositions of the nanodots observed in the sample with $x=0.3$, HRTEM observations presented in Fig. 5 were performed. Consistent with the FESEM results, a mass of nanodots with size of 5–15 nm can be observed. The interplanar distances of several nanodots were measured to be 2.05(5) Å and 1.95(2) Å, which well correspond to the interplanar distances of (1 3 2) and (3 1 1) of ZnSb compound (JCPDS Card 37-1008). Therefore, the aggregation of ZnSb nanostructures can be confirmed by the combination with the results of XRD, DSC, FESEM and HRTEM. Moreover, the peculiar evolution of morphology and size of ZnSb with increasing x from 0.2 to 0.3 may be related to the special nucleation and growth mechanism of ZnSb [19], which is consistent with the XRD results. The Zn substitution as well as the appearance of ZnSb may greatly influence the thermoelectric transport properties, which will be discussed below in detail.

3.2. Electrical transport properties

Fig. 6 displays the temperature dependence of electrical transport properties for the $CeFe_{4-x}Zn_xSb_{12}$ samples. Due to the probable degradation of ZnSb at high temperature as evidenced by DSC curves, the upper measurement temperature of electrical transport properties for the sample with $x=0.3$ is 750 K. As shown in Fig. 6(a), the electrical conductivity decreases monotonically with increasing temperature which indicates a degenerate semiconductor character.

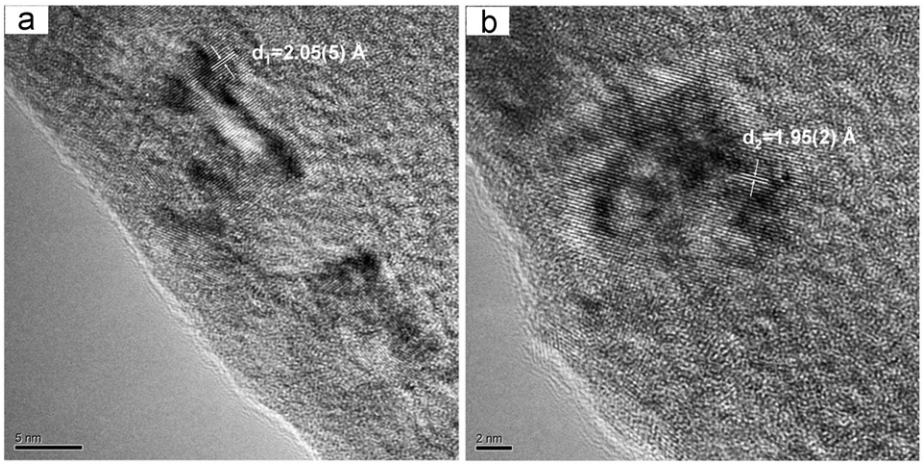

Fig. 5. HRTEM images for the sample $CeFe_{3.7}Zn_{0.3}Sb_{12}$.

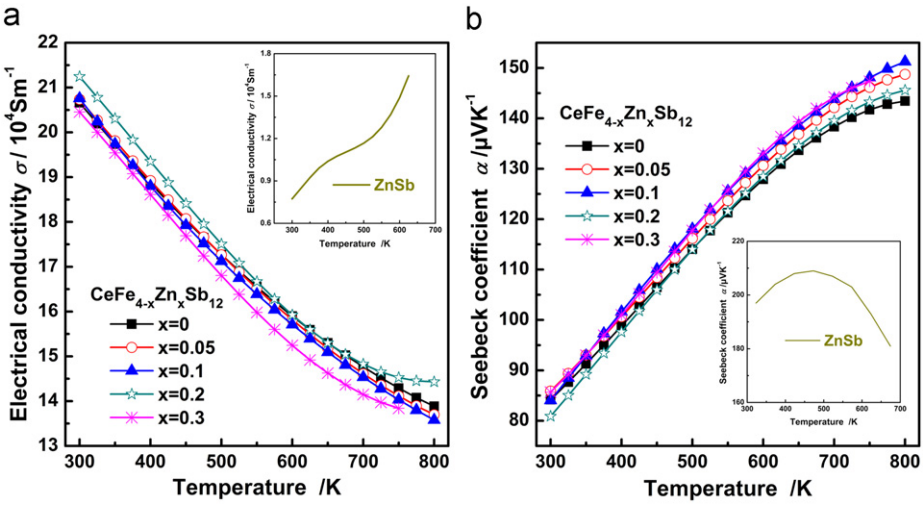

Fig. 6. The temperature dependences of the electrical properties for the $CeFe_{4-x}Zn_xSb_{12}$ compounds. (a) Seebeck coefficient. (b) Electrical conductivity. The insets shown in (a) and (b) display the Seebeck coefficient and electrical conductivity for ZnSb, respectively from Reference [24].

However, for the samples with ZnSb second phase, as can be seen from the insets of Fig. 6(a) and (b), the sign of intrinsic excitation can be clearly observed, which is probably due to the narrow band gap and low electrical conductivity of ZnSb compound [24]. Presumably owing to the isoelectronic substitution, Zn substitution has negligible effect on electrical conductivity in spite of the appearance of ZnSb second phase. In order to further investigate the detailed transport properties of the prepared bulk samples, the room temperature Hall coefficients were measured, and the corresponding carrier concentrations and mobilities were calculated, as summarized in Table 1.

The measured carrier concentrations for all the samples are positive, which indicates that the major carriers are holes. Surprisingly, the carrier concentration increases gradually with increasing Zn content in spite of their isoelectronic nature and lower electronegativity of Zn (1.65) in comparison with that of Fe (1.83). In fact, although many reporters have given the verdict that the valence of Fe is close to 2+ [25], some others argued that a small amount of Fe^{3+} may also exist simultaneously [26]. Therefore, we speculate that Zn substitution may decrease the average valence of Fe to +2 and thus gives an acceptor nature. Moreover, the presumed presence of Sb vacancies originated from the formation of ZnSb would also play an important role in the increase of hole density. The measured Hall mobility decreases with increasing Zn content which is owing to the increased degeneracy with increasing hole concentration or increased interface scattering of ZnSb inclusions. However, the mobility of the sample with $x=0.2$ remains almost unchanged compared with that of the sample with $x=0.1$ in spite of the appearance of ZnSb phase. We speculate that the relatively large ZnSb precipitates with much higher mobility (see Table 1) would have negligible influence on the carrier transport which is dominated by phonon scattering in the vicinity of room temperature. Furthermore, there is a sharp deterioration in mobility for the sample with $x=0.3$ because of the combination of intensified interface scattering by ZnSb nanoinclusions and increased degeneracy owing to the gradual shift of the chemical potential to the heavy valence band.

Fig. 6(b) shows the temperature dependences of Seebeck coefficients for all the samples. The Seebeck coefficients are positive, revealing a p-type conduction, which is consistent with the sign of the Hall coefficient. In addition, it is intriguing that the Zn-substituted samples, showing gradually increased hole concentration with increasing Zn content, possess higher Seebeck

coefficients than that of Zn-free sample. To further understand the mechanisms of the variation in Seebeck coefficient, by assuming a charge carrier scattering distance independent of energy and degenerate approximation, the Seebeck coefficient can be written as Eq. (1) which has also been adopted to calculate the effective mass of other p-type filled skutterudites [14–16]:

$$\alpha = \frac{\pi}{3}\frac{k_B^2 T}{e}\frac{d\ln(\sigma)}{d\ln(E)}\Big|_{E=E_F} = \frac{8\pi^2 k_B^2}{3eh^2} m^* T\left(\frac{\pi}{3N_p}\right)^{2/3} \quad (1)$$

where k_B, E_F, h, m^*, and T are the Boltzmann constant, Fermi energy, Planck constant, effective hole mass and absolute temperature, respectively. The effective mass m^* for all the samples is estimated by Eq. (1) using the measured α and N_p, and is shown in Table 1. It is clear that Zn-substitution significantly increases the value of m^*, which is in good agreement with the decrease in mobility with increasing Zn-substitution amount. The similar phenomenons have also been observed in Cd-doped β-Zn_4Sb_3 and Pd/Ir substituted $Ba_{0.32}Co_4Sb_{12}$ skutterudites [17–19]. Furthermore, the α–N_p plot shown in Fig. 7(a) displays an apparent deviation from Pisarenko relation (shown in the solid line with $m^*=2\ m_e$). In fact, the rare earth filled skutterudites possess unique band structures with the valence band formed by the orbital hybridization among the particular 4f states of fillers, 3d states of transition metals and 5p states of pnictides. The abnormal behavior of carrier concentration dependent Seebeck coefficient can be attributed to the enhancement of density of states effective mass due to the narrow 4f band effects of Ce fillers [27]. Benefiting from the enhanced Seebeck coefficients, as can be seen from Fig. 7(b), the power factors (PF) for the all Zn-substituted samples show some improvements compared with that of the Zn-free sample, especially at elevated temperature.

3.3. Thermal conductivities and ZT values

The total and lattice thermal conductivities as a function of temperature for the samples are presented in Fig. 8. As shown in Fig. 8(a), the total thermal conductivity for all the samples first decreases and then increases with increasing temperature because of bipolar conduction effect. The lattice thermal conductivity κ_L is calculated according to the formula $\kappa_L=\kappa-\kappa_C$, where κ_C is the carrier contribution to thermal conduction calculated according to the Wiedemann–Franz law $\kappa_C=L\sigma T$ with the Lorenz constant L being $2\times10^{-8}\ V^2/K^2$. As can be seen from Fig. 8(b), the lattice thermal conductivity obeys a simple T^{-1} dependence while $T<600$ K due to the domination of phonon–phonon

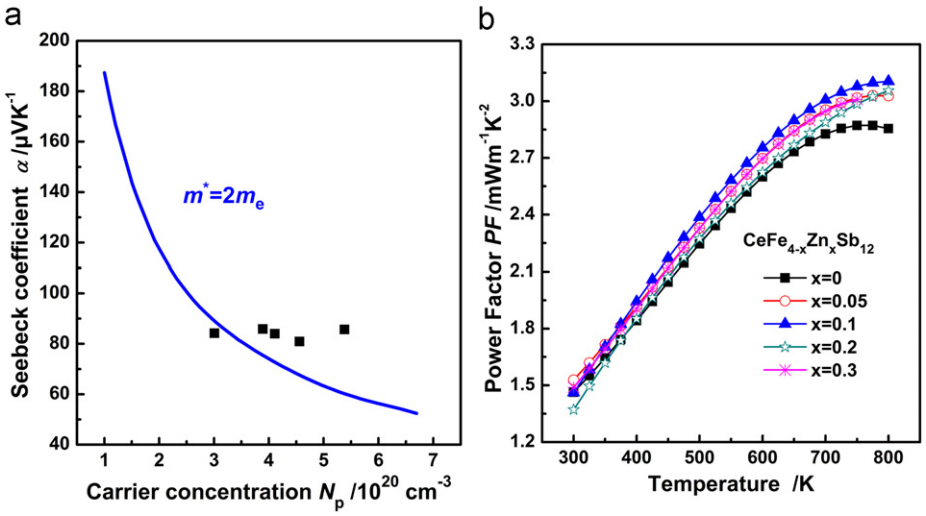

Fig. 7. (a) The measured Seebeck coefficient at room temperature versus carrier concentration for $CeFe_{4-x}Zn_xSb_{12}$ compounds. The solid line indicates a $m^*=2m_e$ relationship. (b) The temperature dependence of power factors for $CeFe_{4-x}Zn_xSb_{12}$ compounds.

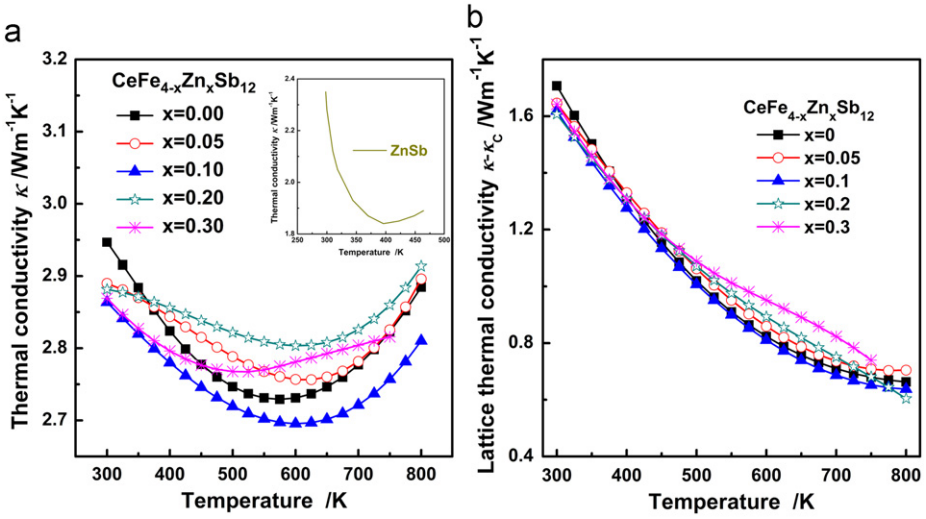

Fig. 8. The temperature dependences of the thermal transport properties for $CeFe_{4-x}Zn_xSb_{12}$ compounds. (a) Thermal conductivity, (b) lattice thermal conductivity.

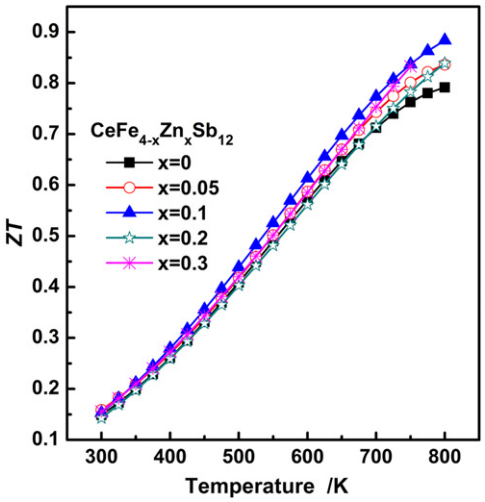

Fig. 9. The temperature dependences of dimensionless figure of merit, *ZT*, for the $CeFe_{4-x}Zn_xSb_{12}$ compounds.

Umlapp process. However, it starts to deviate from such a relationship at elevated temperature ($T>600$ K) owing to the bipolar diffusion. The anomalous temperature dependences of lattice thermal conductivities for the samples with $x=0.2$ and 0.3 can be attributed to the emergence of ZnSb phase which is a narrow band gap semiconductor and shows intrinsic conduction around 400 K, as shown in the inset of Fig. 8(a). Furthermore, the resemblance in κ_L reveals that either Zn-substitution or ZnSb nano-inclusion has negligible influence on the phonon transport behavior. Firstly, owing to the negligible difference in atomic mass between Fe ($M=56$) and Zn ($M=65$), the phonon scattering by mass fluctuation or strain field is insignificant and thus Zn-substitution has a negligible effect on lattice thermal conductivity. Moreover, it is intriguing that the phonon scattering effect caused by nano-inclusions with the size of $\sim$10 nm is inappreciable, which is against the recent results in other thermoelectric material systems [28,32]. The detailed scattering mechanism of phonons in this material needs to be scrutinized.

Fig. 9 displays the temperature dependences of dimensionless figure of merits (*ZT*s) for all the samples. All Zn-doped samples possess higher *ZT* values compared with that of the Zn-free sample, especially at elevated temperature. It is mainly attributed to the enhanced Seebeck coefficients and thus improved power factors. The maximum *ZT* value reaches 0.9 at 800 K for the sample with $x=0.1$, which is about 15% improvement over the Zn-free sample. This improvement in *ZT* unambiguously demonstrates that Zn-substitution is an effective approach to improve the thermoelectric properties of p-type Fe-based skutterudites. In addition, a further enhancement in *ZT* can be expected by combining some other techniques, such as multiple filling, crystal grains refinement and introduction of other structural disorder.

4. Conclusions

In summary, p-type Ce fully filled and Zn-substituted skutterudites, $CeFe_{4-x}Zn_xSb_{12}$ ($x=0$, 0.05, 0.1, 0.2, 0.3), have been successfully prepared by a traditional melting–annealing–spark plasma sintering method in this study. The solubility limit of Zn in the Fe site is proved to be around 0.12, exceeding which ZnSb nano-inclusions will emerge. The Seebeck coefficient is anomalously enhanced by the introduction of Zn, whereas Zn-substitution and/or ZnSb nano-inclusions have negligible influences on both electrical and thermal conductivity. As a result, the *ZT* values of Zn-substituted samples are improved greatly in comparison with that of Zn-free sample. The maximum *ZT* value reaches 0.9 at 800 K for the sample with $x=0.1$, which is about 15% improvement over the Zn-free sample.

Acknowledgments

This work was partially supported by the Natural Science Foundation of China Grant Nos. 51172174 and 51002112) and International Science & Technology Cooperation Program of China (Grant No. 2011DFB60150) along with 111 Project (Grant No. B07040).

References

[1] D.T. Morelli, G.P. Meisner, J. Appl. Phys. 77 (1995) 3777–3781.
[2] D.T. Morelli, G.P. Meisner, B.X. Chen, S.Q. Hu, C. Uher, Phys. Rev. B 56 (1997) 7376–7383.
[3] Y.Z. Pei, L.D. Chen, W. Zhang, X. Shi, S.Q. Bai, X.Y Zhao, Appl. Phys. Lett. 89 (2006) 221107.
[4] L.D. Chen, T. Kawahara, X.F. Tang, T. Goto, T. Hirai, J.S. Dyck, W. Chen, C. Uher, J. Appl. Phys. 90 (2001) 1864–1868.
[5] J. Eilertsen, J. Li, S. Rouvimov, M.A. Subramanian, J. Alloys Compd. 509 (2011) 6289–6295.
[6] V.L. Kuznetsov, L.A. Kuznetsova, D.M. Rowe, J. Phys. Condens. Matter 15 (2003) 5035–5048.
[7] M. Puyet, B. Lenoir, A. Dauscher, M. Dehmas, C. Stiewe, E. Muller, J. Appl. Phys. 95 (2004) 4852–4855.
[8] M. Puyet, B. Lenoir, A. Dauscher, P. Weisbecker, S.J. Clarke, J. Solid State Chem. 177 (2004) 2138–2143.
[9] X. Shi, W. Zhang, L. Chen, J. Yang, C. Uher, Acta Mater. 56 (2008) 1733–1740.
[10] J. Yang, Y. Chen, W. Zhu, J. Peng, S. Bao, X. Fan, X. Duan, J. Solid State Chem. 179 (2006) 212–216.
[11] G. Rogl, A. Grytsiv, P. Rogl, E. Bauer, M. Zehetbauer, Intermetallics 19 (2011) 546–555.
[12] G.A. Slack., in: DM Rowe (Ed.), CRC Handbook of Thermoelectrics, CRC, Boca Raton, FL, 1995, p. 407.
[13] P.F. Qiu, J. Yang, R.H. Liu, X. Shi, X.Y. Huang, G.J. Snyder, W. Zhang, L.D. Chen, J. Appl. Phys. 109 (2011) 063713.
[14] R. Liu, X. Chen, P. Qiu, J. Liu, J. Yang, X. Huang, L. Chen, J. Appl. Phys. 109 (2011) 023719.
[15] R.H. Liu, P.F. Qiu, X.H. Chen, X.Y. Huang, L.D. Chen, J. Mater. Res. 26 (2011) 1813–1819.
[16] R.H. Liu, J. Yang, X.H. Chen, X. Shi, L.D. Chen, C. Uher, Intermetallics 19 (2011) 1747–1751.
[17] Y.Z. Pei, L.D. Chen, X.Y. Zhao, W.Q. Zhang, X.Y. Li, T. Goto, Appl. Phys. A 85 (2006) 451–455.
[18] Y.Z. Pei, L.D. Chen, S.Q. Bai, X.Y. Zhao, X.Y. Li, Scr. Mater. 56 (2007) 621–624.
[19] S.Y. Wang, H. Li, D.K. Qi, W.J. Xie, X.F. Tang, Acta Mater. 59 (2011) 4805–4817.
[20] G.S. Nolas, V.G. Harris, T.M. Tritt, G.A. Slack, J. Appl. Phys. 80 (1996) 6304–6308.
[21] T. Caillat, J. Kulleck, A. Borshchevsky, J.P. Fleurial, J. Appl. Phys. 79 (1996) 8419–8426.
[22] L. Pan, X.Y. Qin, H.X. Xin, D. Li, J.H. Sun, J. Zhang, C.J. Song, R.R. Sun, Intermetallics 18 (2010) 1106–1110.
[23] V. Lzard, M.C. Record, J.C. Tedenac, S.G. Fries, Calphad 25 (2001) 567–581.
[24] L.T. Zhang, M. Tsutsui, K. Ito, M. Yamaguchi, J. Alloys Compd. 358 (2003) 252–256.
[25] A.P. Grosvenor, R.G. Cavell, A. Mar, Chem. Mater. 18 (2006) 1650–1657.
[26] D. Jung, M.H. Whangbo, S. Alvarez, Inorg. Chem. 29 (1990) 2252–2255.
[27] Hiroaki Anno, Jiro Nagao, KakueiMatsubara, Proceedings of the 21st International Conference on Thermoelectrics, 2002, CA, USA, pp.56–59.